New insights into the crystal structure of UTE0.25Ge2=U4TGe8 (TE = Ru, Os) and ferromagnetic properties of the Os-bearing uranium germanide

Graziella Guy, Maria Szlawska, Carmelo Prestipino, Vincent Dorcet, Valérie Demange, Pierre Fertey, Dariusz Kaczorowski, Mathieu Pasturel, Adam Pikul

New insights into the crystal structure of $UTE_{0.25}Ge_2 = U_4TGe_8$ (*TE* = Ru, Os) and ferromagnetic properties of the Os-bearing uranium germanide.

Graziella Guy,[1] Maria Szlawska,[2] Carmelo Prestipino,[1] Vincent Dorcet,[1] Valérie Demange,[1] Pierre Fertey,[3] Dariusz Kaczorowski,[2] Mathieu Pasturel,[1,*] Adam Pikul[2]

[1] *Univ Rennes, CNRS, Institut des Sciences Chimiques de Rennes – UMR6226, ScanMAT – UAR2025, 35042 Rennes, France*

[2] *Institute of Low Temperature and Structure Research, Polish Academy of Sciences, ul. Okólna 2, 50-422 Wrocław, Poland*

[3] *Synchrotron Soleil, CRISTAL beamline, L'Orme des Merisiers, 91190 Saint-Aubin, France*

* corresponding author: mathieu.pasturel@univ-rennes1.fr

Abstract

A single crystal of the compound previously described as "$URu_{0.25}Ge_2$" was studied by means of transmission electron microscopy and synchrotron X-ray diffraction (XRD) measurements. The experiments revealed that the deficient ruthenium atoms order to a superstructure of the $CeNiSi_2$ structure-type with space group $P2_1/n$ (no. 14) and cell parameters a' = 5.7422(7) Å, b' = 15.931(2) Å, c' = 11.4903(9) Å and β' = 90.755(8)°, corresponding to the Tb_4FeGe_8-type structure. In addition, a new isostructural compound U_4OsGe_8 was synthesized and characterized by powder X-ray diffraction, electron diffraction, DC magnetization, AC susceptibility, electrical resistivity and specific heat measurements. The experiments showed that it crystallizes with the monoclinic, ordered $P2_1/n$ unit cell with lattice parameters a' = 5.7438(1) Å, b' = 15.9355(1) Å, c' = 11.4586(1) Å and β' = 90.681(1)°, and orders ferromagnetically at about 54 K, which is clearly seen in all the physical properties studied. Moreover, its electrical resistivity was found to exhibit features characteristic of semimetals, and the electron contribution to the specific heat is moderately enhanced, as in all other known phases of the $UTE_{1-x}Ge_2$ (with *TE* = transition element) family of compounds.

Keywords

Uranium germanides; electron and synchrotron X-ray diffraction; magnetic and related properties; ordered vacancies; ferromagnetism.

Introduction

Binary and ternary uranium germanides form a broad family of intermetallics with a wide range of crystallographic and physical properties, with unit cell volumes ranging from tens to several thousand Å^3 (*e.g.* $U_{34}Fe_{4-x}Ge_{33}$ [1] or $U_9Fe_7Ge_{24}$ [2]), with magnetic behavior changing from Pauli paramagnetism (*e.g.* UFe_2Ge_2 [3], $U_6Co_{12}Ge_4$[4], $U_3Co_{12}Ge_4$ [5], $U_4Os_7Ge_6$ [6]) to hard ferromagnetism (*e.g.* UGe_2 [7], U_3TiGe_5 [8], $U_3Fe_2Ge_7$ [9], $U_3Cu_4Ge_4$ [10]). Among these properties, very exotic ones are reported, such as ferromagnetic (FM) ordering despite very short U-U distances in U_2Fe_3Ge [11,12] or the coexistence of a FM order with superconductivity (SC) in UGe_2 [13], UCoGe [14] and URhGe [15]. The presence of U-zigzag chains in the latter 3 examples seems to be of uttermost importance for the local inversion symmetry breaking in the FM ordered state and the formation of the SC state [16].

The recently reported $UTE_{1-x}Ge_2$ family crystallizes in the orthorhombic (*TE* = Fe [17,18], Co [19], Ni [20-23]) or slightly monoclinically distorted (*TE* = Ru [24]) $CeNiSi_2$ structure-type strongly related to that of UGe_2 [24]. In particular, in these structure-types, U-atoms form almost identical zigzag chains resulting from the formation of almost identical layers of Ge-centered [U_6] trigonal prisms separated by planar layers of Ge-atoms, without (in UGe_2) or with (in $UTE_{1-x}Ge_2$) partial intercalation of the transition element *TE* on either side of this planar layer. As a likely consequence of this structural relationship, these germanides exhibit ferromagnetic (T_C = 52, 37, 63, and 18 K for UGe_2 and $UTE_{1-x}Ge_2$ with *TE* = Fe, Ru and Co, respectively) or antiferromagnetic ordering with FM coupling within the [U_6] layers (T_N = 47 K for T = Ni).

An upturn of the electrical resistivity at the lowest measured temperatures clearly demonstrates the absence of superconductivity in the $UTE_{1-x}Ge_2$ series [17,22,24], at least at ambient pressure. It has been suggested that this upturn is due to the crystallographic disorder induced by the partly occupied transition metal site. However, (i) studies report on ordered *TE* vacancies leading to the formation of superstructures in ternary rare-earth germanides based on the same deficient structure-type [25-27] and (ii) the 1-*x* values found in these compounds is close to ½, ⅓ and ¼. Such observations have prompted us to re-examine their crystal structure using more sensitive techniques than regular laboratory X-ray diffraction (XRD), and to demonstrate whether the formation of superstructures resulting from the ordered occupancy of the transition metal site is possible or not. Since selected area electron diffraction using a transmission electron microscope (TEM) has been shown to be an effective tool for evidencing vacancy ordering and subsequent superstructure formation in intermetallic compounds (see *e.g.* [25-30]), it was used in the present study. These analyses have been complemented by single crystal Synchrotron XRD to *ab initio* determine the crystal structure. In this article, we present the results of the experiments performed on "$URu_{0.29}Ge_2$"

(preliminary characterization of which was outlined in Ref. 23) and another member of this series – "$UOs_{0.25}Ge_2$", supplemented by results of magnetic, electrical and specific heat properties measurements of the latter novel phase.

Experimental details

The previously described "$URu_{0.25}Ge_2$" sample [24] was used for transmission electron microscopy and synchrotron X-ray diffraction (XRD) experiments. The "$UOs_{0.25}Ge_2$" sample was synthesized using the same procedure, *i.e.* by arc-melting followed by annealing at 1073 K for two weeks.

The products were characterized by powder XRD using a Bruker Advance D8 diffractometer (Cu Kα1 radiation, λ = 1.5406 Å) and scanning electron microscopy (SEM, Jeol JSM 7100F) coupled to energy dispersive spectroscopy (EDS, Oxford SDD X-max spectrometer). XRD patterns were analyzed using the Rietveld method implemented in the FullProf program [31].

Selected-area electron diffraction was performed on a Jeol 2100 LaB_6 transmission electron microscope (TEM) operating at 200 kV. For these analyses, the samples were ground to fine powder by hand hammering them in dry ethanol using an agate mortar, and droplets of the obtained suspension were deposited on carbon-coated copper grids.

Single crystal of U_4RuGe_8 extracted from the polycrystalline sample "$URu_{0.25}Ge_2$" was measured in a double-closed sample holder on the CRISTAL beamline at the SOLEIL synchrotron mounted on an in-vacuum U20 undulator. The beamline is equipped with a Newport four-circle k diffractometer, equipped with an Oxford Diffraction Atlas CCD detector. Approximately 8000 reflections were collected at a wavelength of 0.67093 Å. Data integration was performed using the CrysAlis^{Pro} suite (*CrysAlis^{Pro}*, Oxford Diffraction /Agilent Technologies UK Ltd, Yarnton, England). The structure was solved *ab initio* using the charge flipping algorithm [32] and successively refined using the Jana2006 software [33]. Crystallographic data standardization was performed using the STIDY program [34]. Notice, rather elevated reliability factor values are attributed to the combined effect of the high X-ray absorption coefficient of crystals and increase in background due to the double-confinement layers.

The *dc* magnetization of the U_4OsGe_8 sample was measured in the temperature range 1.72–300 K and in magnetic fields up to 70 kOe using a Quantum Design MPMS-7 superconducting quantum interference device (SQUID) magnetometer. Heat capacity was measured between 2 and 300 K and up to 30 kOe by a temperature relaxation method using a Quantum Design PPMS-9 platform. The same apparatus was used to measure the electrical resistivity down to 2 K and up to 30 kOe using the standard four-point technique.

Results and discussion

Crystal structures of U_4TEGe_8 (*TE* = Ru and Os)

Typical electron diffraction patterns of "$URu_{0.25}Ge_2$" and "$UOs_{0.25}Ge_2$" collected along selected zone axes are shown in fig. SI1 and 1, respectively. The most intense diffraction peaks can be well indexed with the monoclinic unit cell reported for $URu_{0.29}Ge_2$ (*C*2/*c* space-group and cell parameters a = 4.098 Å, b = 15.936 Å, c = 4.045 Å and β = 90.091°). However, less intense diffraction peaks are observed (blue arrows in fig. 1), indicating the formation of a superstructure, propagating in the (*a*,*c*) plane of the initial cell. The home-developed TEMpcPlot software [35] was used to index all diffraction spots and determine the approximative parameters of the supercell: $a' \approx 5.9$ Å, $b' \approx 16.3$ Å, $c' \approx 11.9$ Å and $\beta' \approx 90.7°$. These values of the a' and c' parameters correspond roughly to a single and double length of the diagonal of the basal plane of the initial unit cell (fig. 2), leading to a fourfold increase in the supercell volume. In addition, to the initial stoichiometry of these germanides ($1-x \approx ¼$), one can easily imagine a U_4TEGe_8 composition for these compounds.

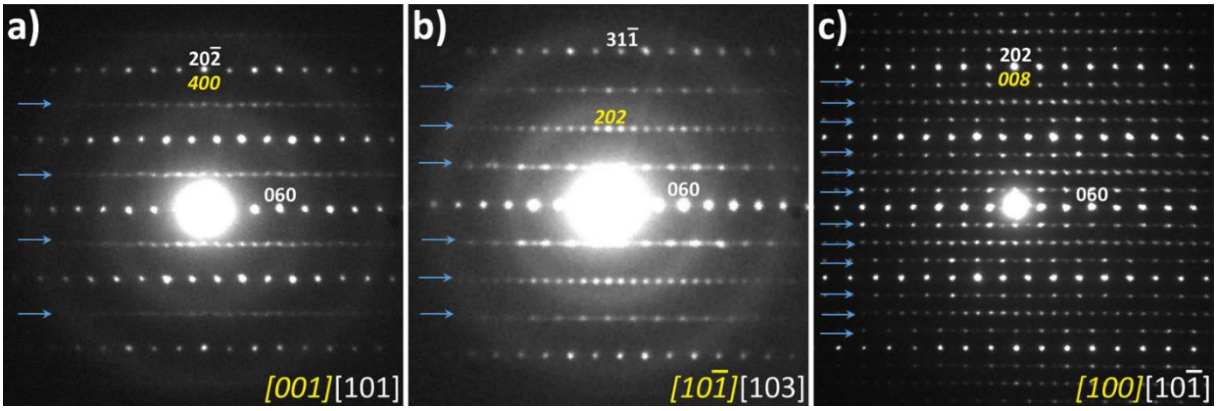

Figure 1 Selected SAED patterns of U_4OsGe_8 along different zone axes, indexed in the disordered monoclinic derivative of the $CeNiSi_2$-type structure (white) and in the ordered Tb_4FeGe_8-type superstructure (yellow).

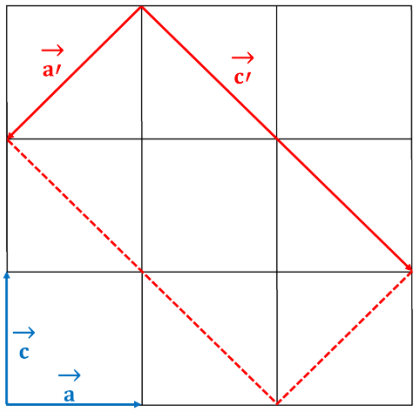

Figure 2 Comparison of the unit cells of the disordered monoclinic derivative of the $CeNiSi_2$-type of structure (blue) and the ordered Tb_4FeGe_8-type superstructure (red). In both cases, the *b*-axis is directed perpendicularly downward in the figure.

Single crystal XRD was therefore performed on the Ru-bearing phase at CRISTAL beamline of the Soleil synchrotron. The superstructure with the space group $P2_1/n$ (no. 14) and supercell parameters a' = 5.7422(7) Å, b' = 15.931(2) Å, c' = 11.4903(9) Å and β' = 90.755(8)° was confirmed. The crystal structure solution and refinements (see tables 1 & 2) indicate 13 independent atomic positions in the cell: four *4e* sites for U-atoms, one *4e* site for Ru-atom and eight *4e* sites for Ge-atoms, confirming the U_4RuGe_8 stoichiometry. This structure thus corresponds to the ordered Tb_4FeGe_8-type reported by Zhuravleva *et al.* [25]. Normalization of the crystallographic data leads to the $P2_1/c$ (no. 14) space group with a'' = 5.7422(7) Å, b'' = 15.931(2) Å, c'' = 12.777(1) Å and β'' = 115.95(1)° and the atomic positions presented in tables 1 & 2. The group-subgroup relations from orthorhombic *Cmcm* $CeNiSi_2$-type to this standardized monoclinic $P2_1/c$ Tb_4FeGe_8-type are shown in fig. SI2. For comparison with the latter study, we will use the description of the $P2_1/n$ structure in the following.

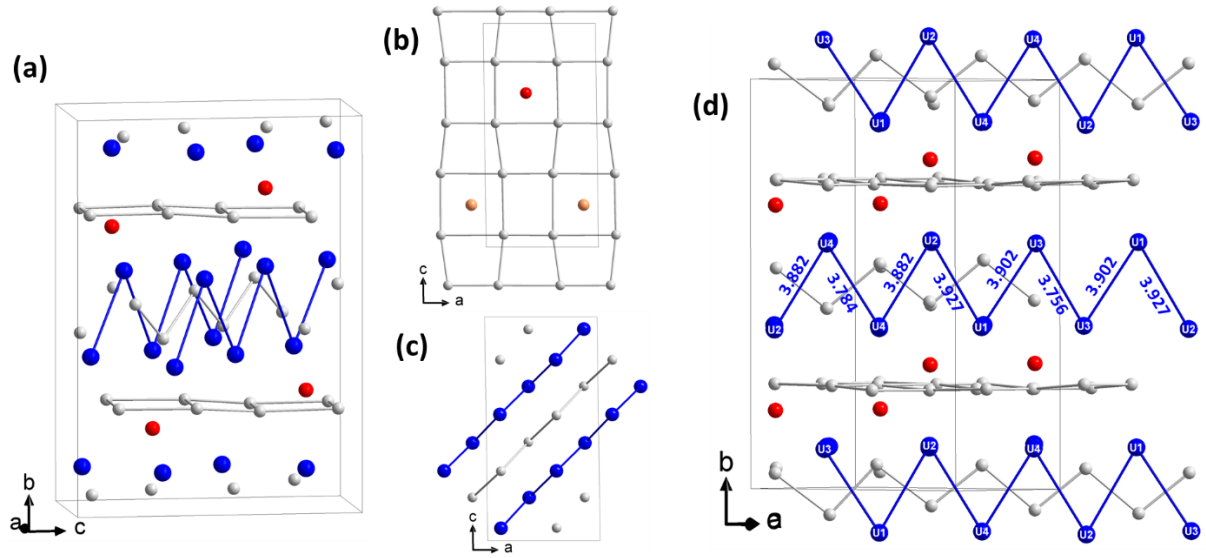

Figure 3 (a) Perspective view of the crystal structure of U_4RuGe_8 with U, Ru and Ge atoms represented as blue, red, and grey balls, respectively. (b,c) Projections of selected layers of this crystal structure along the *b*-axis, showing the distorted [Ge_4] network and the propagation direction of the U zigzag chains, respectively. Red and pink spheres stand for Ru atoms located above and below the [Ge_4] layer, respectively. (d) Structure projection highlighting the various U-U distances along the zigzag chains.

This structure-type is an ordered derivative of the deficient $CeNiSi_2$ one, where the ordered occupancy of Ru-atoms in the supercell induces distortions of the germanium sublattice (fig. 3) which were not detected from the previous XRD measurements but are probably necessary to accommodate the local strains induced by the presence of the transition metal [25-27]. Consequently, the Ge-layers separating the [U6] trigonal prisms layers are no more planar, and the [Ge_4] quadrilaterals are no more "square-like", showing trapezoidal or rectangular features (fig. 3b). The layers of the Ge-centered [U_6] trigonal prisms are somewhat less affected by the presence of Ru and only small distortions are visible in the supercell compared to the average one, leading to various U-U distances along the chains

spreading from 3.756(1) to 3.9275(9) Å and angles from 61.52(2)° to 63.91(2)° (fig. 3d). In contrast to the case of Tb_4FeGe_8, one single *4e* atomic position was found for Ru-atoms instead of two, partly occupied, for Fe-atoms.

Table 1 Single crystal synchrotron X-ray diffraction data collection and refinement parameters for U_4RuGe_8

Empirical formula	U_4RuGe_8	
	Zhuravleva's setting [25]	Standardized data
Formula weight (g mol^{-1})	1633.9	
Structure-type	Tb_4FeGe_8	
Space group	$P2_1/n$ (14)	$P2_1/c$ (14)
Unit cell parameters (Å)	a' = 5.7422(7) Å	a'' = 5.7422(7) Å
	b' = 15.931(2) Å	b'' = 15.931(2) Å
	c' = 11.4903(9) Å	c'' = 12.777(1) Å
	β' = 90.755(8)°	β'' = 115.95(1)°
Unit cell volume (Å^3)	1051.0(2)	
Z / calculated density (g cm^{-3})	4 / 10.33	
Radiation / wavelength (Å)	Synchrotron, 0.67093	
Absorption coefficient (mm^{-1})	22.018	
Theta range	2.06° - 32.25°	
Limiting indices	$-9 \le h \le 8$ $-23 \le k \le 23$ $-18 \le l \le 18$	
Collected/unique reflections	8151/8136	
Absorption correction	Multi-scan	
T_{min} / T_{max}	0.49 / 1	
Data / restraints / parameters	8136/0/120	
Goodness of fit on F²	1.9458	
R indices [I>2σ(I)]	R = 0.0492 wR_2 = 0.0571	
Largest difference peak and hole (e Å^{-3})	5.12 / -5.50	

Using this structural model, Rietveld refinements of the powder XRD patterns of the Ru- and Os-bearing phases were carried out (fig. SI3 & SI4, tables SI1). The agreement for U_4RuGe_8 is very good, and most of the low intensity peaks previously attributed to the large unit cell of $U_9Ru_7Ge_{24}$ are indexed within the Tb_4FeGe_8 structure type. In the case of U_4OsGe_8, for which no suitable single crystal was found, the Bragg peak positions are well indexed with cell parameters a' = 5.7438(1) Å, b' = 15.9355(1) Å, c' = 11.4586(1) Å and β' = 90.681(1)°. Nevertheless, while the overall peak intensity ratio is well described with the single crystal model determined for U_4RuGe_8, some intensity mismatches are observed, indicating the need to adjust some atomic positions for U_4OsGe_8. However, the large number of adjustable parameters (3 × 13 atoms) leads to quite unstable refinements, making it difficult to definitively conclude about precise atomic positions in the unit cell. In both cases, lowering the symmetry to triclinic *P*-1 space-group and using the Y_4RuGe_8 structure-type reported by Bao *et al.* [27] does not significantly improve the quality of the refinements. Moreover, the smaller Bragg peaks

calculated for this triclinic unit cell are strongly offset from the experimental observations, ruling out this hypothetical superstructure in the here discussed cases.

Both XRD (fig. SI4) and SEM-EDS analyses (fig. SI5 and table SI2) indicate the presence of about 6 wt.% of UGe_3 as an impurity in the U_4OsGe_8 sample. This phase being paramagnetic will not significantly affect the physical properties of the major phase described below.

Table 2 Refined atomic coordinates and isotropic displacement parameters for U_4RuGe_8, obtained from synchrotron X-ray diffraction data, and presented in both published and standardized settings.

	Zhuravleva's setting ($P2_1/n$) [25]					Standardized setting ($P2_1/c$)			
Atom	Wyck.	x'	y'	z'	U_{eq} (10^{-3} Å^2)	Wyck.	x''	y''	z''
U1	*4e*	0.8794(2)	0.38584(3)	1.18863(9)	7.6(2)	*4e*	0.5533(2)	0.09985(4)	0.43338(8)
U2	*4e*	-0.1231(2)	0.39139(3)	0.68737(9)	8.3(2)	*4e*	0.3105(2)	0.39139(3)	0.18737(9)
U3	*4e*	-0.1192(2)	0.10194(4)	0.44267(8)	7.8(2)	*4e*	0.0618(2)	0.39806(4)	0.44267(8)
U4	*4e*	0.3799(2)	0.40015(4)	0.43328(8)	8.1(2)	*4e*	0.1908(2)	0.60416(3)	0.31137(9)
Ru1	*4e*	0.8768(3)	0.19402(6)	0.6871(2)	9.5(3)	*4e*	0.3103(3)	0.19402(6)	0.1871(2)
Ge1	*4e*	0.5992(4)	0.2559(2)	0.5502(2)	16.6(6)	*4e*	0.4510(5)	0.2559(2)	0.0502(2)
Ge2	*4e*	0.3704(6)	0.4397(1)	0.6895(3)	11.5(4)	*4e*	0.8191(6)	0.4397(1)	0.1895(3)
Ge3	*4e*	0.6233(6)	0.53954(9)	0.8098(3)	10.1(4)	*4e*	0.3135(6)	0.03954(9)	0.1902(3)
Ge4	*4e*	0.1562(3)	0.2569(2)	0.5511(2)	11.2(5)	*4e*	0.1051(4)	0.7569(2)	0.4489(2)
Ge5	*4e*	-0.1235(5)	0.4469(2)	0.4393(2)	11.3(5)	*4e*	0.0628(6)	0.0531(2)	0.4393(2)
Ge6	*4e*	0.1022(4)	0.2443(1)	0.3273(2)	12.3(5)	*4e*	0.2749(4)	0.7557(1)	0.1727(2)
Ge7	*4e*	-0.3442(3)	0.2445(1)	0.3272(2)	8.5(5)	*4e*	0.1714(3)	0.2555(1)	0.3272(2)
Ge8	*4e*	0.8843(6)	0.4416(2)	0.9422(2)	11.2(6)	*4e*	0.5579(6)	0.4416(2)	0.4422(2)

Physical properties of $UOs_{0.25}Ge_2$

Magnetic properties

The results of magnetic properties measurements of the polycrystalline sample of U_4OsGe_8 are gathered in Fig. 4. The main panel displays the temperature dependence of the inverse molar magnetic susceptibility χ^{-1}. Above 120 K, the $\chi^{-1}(T)$ curve can be described by the modified Curie-Weiss law in a form:

$$\chi(T) = \chi_0 + (\mu^2_{eff}/8)/(T - \theta_P), \quad (1)$$

where μ_{eff} is the effective magnetic moment, θ_P stands for the paramagnetic Curie temperature, and χ_0 is a sum of temperature independent contributions. By fitting the equation to the experimental data, the following parameters were obtained: μ_{eff} = 2.6 μ_B, θ_P = 39 K, and χ_0 = 5 10^{-4} emu mol_U^{-1}. The value of μ_{eff} is smaller than that expected for free trivalent U^{3+} and tetravalent U^{4+} ions (3.62 and 3.58 μ_B, respectively). The reduction can be attributed to partial delocalization of uranium 5*f* electrons,

magnetocrystalline anisotropy and/or crystal field effect. The positive value of θ_P indicates predominant ferromagnetic character of the exchange correlations between U ions.

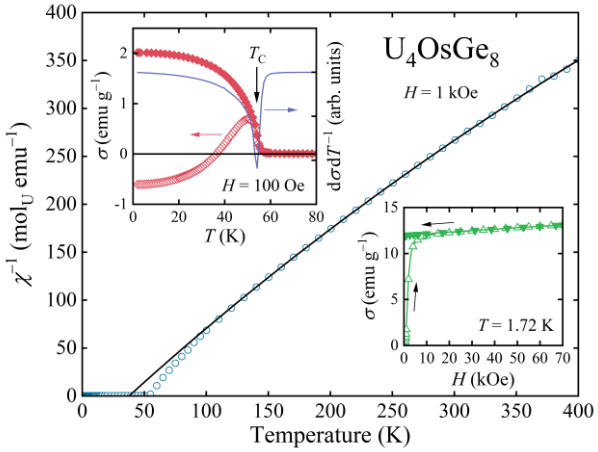

Figure 4 Inverse magnetic susceptibility of polycrystalline sample of U_4OsGe_8 measured as a function of temperature in a constant magnetic field *H* of 1 kOe. The solid line shows the fit of Eq.(1) to the experimental data. Upper inset shows the low-temperature dependence of the mass magnetization σ in zero-field-cooled (open symbols) and field-cooled regimes (closed symbols); solid line is the temperature derivative of $\sigma(T)$ measured in the field-cooled regime. Lower inset shows $\sigma(H)$ measured at a constant temperature of 1.72 K with increasing (open symbols) and decreasing field (closed symbols); solid curves serve as guides for the eyes.

The upper inset to Fig. 4 shows the low-temperature variations of the magnetization σ of U_4OsGe_8 measured in a constant magnetic field of 100 Oe after cooling the sample down in zero and finite magnetic field (*i.e.* in the ZFC and FC regimes). A pronounced anomaly in $\sigma(T)$ at about 54 K (*cf.* the temperature derivative of $\sigma(T)$) clearly manifests the occurrence of magnetic ordering, and a Brillouin-like shape of the curve measured in the FC regime points to its long-range ferromagnetic nature, in line with the positive value of θ_P. Pronounced bifurcation between the ZFC and FC curves, and a negative sign of $\sigma(T)$ measured at low temperature in the ZFC mode can be ascribed to the presence of ferromagnetic domains in the ordered state.

The field dependence of the magnetization, $\sigma(H)$, measured deep in the magnetically ordered region with increasing and decreasing magnetic field, corroborates the ferromagnetic order. In weak fields, the magnetization increases rapidly and exhibits a clear tendency toward saturation already above about 1 kOe. In the strongest applied magnetic field (*i.e.* 70 kOe) it reaches a value of 13.08 emu g^{-1} which corresponds to the ordered magnetic moment of about 1 μ_B, that is very close to the values reported for other $UTE_{1-x}Ge_2$ compounds [22-24]. With decreasing magnetic field, the magnetization decreases in a linear manner, down to the remnant value as large as about 12 emu g^{-1}. Nevertheless, the hysteresis loop of U_4OsGe_8 is rather narrow.

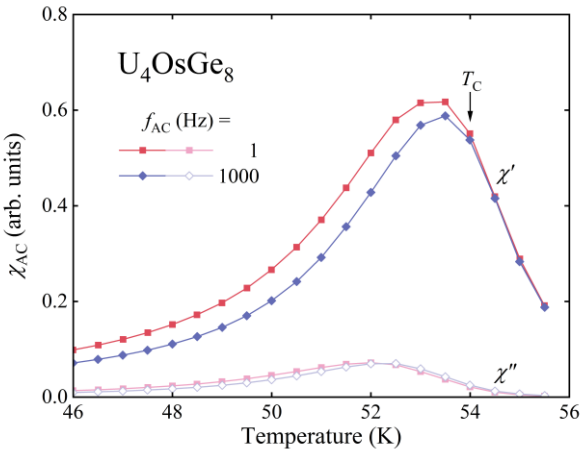

Figure 5 Real and imaginary components of the *AC* susceptibility χ_{AC} of U_4OsGe_8 (χ' and χ'', respectively) measured near the Curie temperature T_C in a probing AC field of 3.7 Oe oscillating with the frequency f_{AC} of 1 and 1000 Hz; solid lines serve as guides for the eye.

The ferromagnetic character of the ordering in U_4OsGe_8 is further confirmed by the AC magnetic susceptibility measurements (Fig. 5). Both components of the AC susceptibility, real and imaginary, form distinct maxima, located slightly below the Curie temperature derived from the DC magnetization data. The position of the maxima does not change significantly with an increase in the frequency of the probing magnetic field, which is expected for long-range-ordered ferromagnets.

Electrical resistivity

The temperature dependence of the electrical resistivity ρ of U_4OsGe_8 is shown in Fig. 6. At room temperature the resistivity has a fairly large value of 517 μΩ cm and only slightly decreases with decreasing temperature down to the ferromagnetic transition, forming a very wide hump characteristic of uranium intermetallics. Below T_C, the $\rho(T)$ curve shows a faint maximum followed by significantly faster decrease in ρ with lowering T due to rapid reduction in scattering conduction electrons on the ferromagnetically aligned magnetic moments. At the lowest temperature available in the experiment (*i.e.* 2 K) the resistivity reaches approximately 250 μΩ cm, leading to the residual resistivity ratio RRR = ρ(300 K)/ρ(2 K) of only about 2. The temperature variation of the electrical resistivity of U_4OsGe_8 can be compared with the data reported for the other $UTE_{1-x}Ge_2$ germanides. For all of them, ρ has rather high magnitude and weak temperature dependence, but those with disordered crystal structure (*i.e.* with *TE* = Ni) show the lowest RRR values [22].

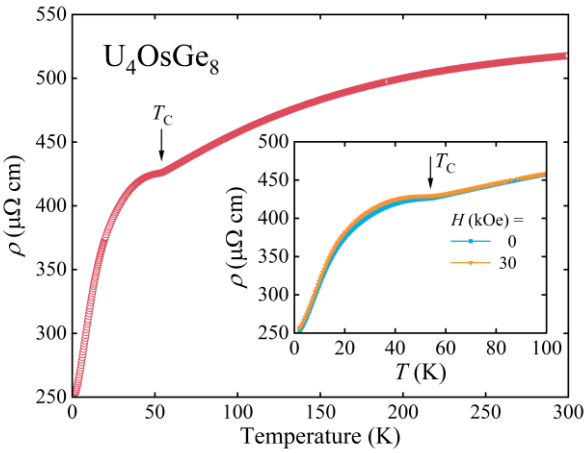

Figure 6 Temperature dependence of electrical resistivity ρ of U_4OsGe_8. Inset: ρ (T) below 100 K measured in various magnetic fields.

Another feature that is common to the whole family of the $UTE_{1-x}Ge_2$ compounds is the increase in the resistivity or the formation of a small resistivity maximum below the magnetic ordering temperature, regardless of the type of the ordering [7,24]. Remarkably, very similar shape of ρ(T) near the Curie temperature, has also been reported for UGe_2 measured along the *b* axis of its orthorhombic unit cell [7,36]. This behavior may suggest that the magnetic structure of U_4OsGe_8 is more complex than a simple colinear ferromagnetic arrangement of uranium magnetic moments. However, this is rather unlikely, since the magnetic structure of at least one member of the $UTE_{1-x}Ge_2$ family, namely that with Ni [22,23], is in fact very simple and colinear, while its resistivity shows very similar characteristics to that of U_4OsGe_8. Moreover, as can be inferred from the inset to Fig. 6, the magnetic field has almost no effect on the electrical resistivity of U_4OsGe_8 at least up to 30 kOe. Strictly speaking, only a barely visible change in the position of the anomaly at T_C and a tiny reduction of ρ in the ordered region is noticeable in the applied field. Notice, the presence in our sample of UGe_3 impurity which is reported to have a metallic behaviour with 10 times smaller resistivity values over the whole studied temperature range (see *e.g.* [37]) do not seem to influence significantly the measurements.

The electrical transport properties of the $UTE_{1-x}Ge_2$ compounds, *i.e.* (i) large magnitude of the resistivity, (ii) weak temperature variation of $\rho(T)$, (iii) small RRR, observed regardless of the presence of any significant crystallographic disorder, and (iv) increase of the resistivity below T_C unrelatedly to the type of the magnetic ordering, clearly indicate their semi-metallic nature.

Specific heat

Fig. 7 shows the temperature dependence of the specific heat C_p of U_4OsGe_8 measured in zero magnetic field. At room temperature, the specific heat reaches a value of about 336 J K^{-1} mol^{-1}, which

is close to the Dulong-Petit limit of $3nR$ = 324 J K^{-1} mol^{-1}, where n = 13 is the number of atoms per formula unit and R = 8.315 J K^{-1} mol^{-1} is the universal gas constant.

As displayed in Fig. 7, the experimental $C_P(T)$ curve can be reasonably well approximated down to about 100 K by the formula:

$$C_P = \gamma^{\mathrm{HT}} T + 9nR \left(\frac{T}{\Theta_D^{\mathrm{HT}}}\right)^3 \int_0^{\Theta_D^{\mathrm{HT}}/T} \frac{x^4 e^x}{(e^x-1)^2} dx, \qquad (2)$$

where the first term is the electron contribution to C_P with the Sommerfeld coefficient γ^{HT}, and the second one represents the lattice contribution to C_P with the characteristic Debye temperature Θ_D^{HT}. (the superscript HT indicates high-temperature range of $C_P(T)$ being considered). The least-squares fits of Eq. (2) to the experimental data yielded the parameters γ^{HT} = 76 mJ mol^{-1} K^{-2} (or 19 mJ mol$_U^{-1}$ K^{-2}) and Θ_D^{HT} = 259 K. It should be noted that in the HT description of $C_P(T)$ in terms of Eq. 2 we deliberately neglected Schottky term due to the crystal field effect. Our approach can be justified by the fact that the latter contribution to $C_P(T)$ is incomparably smaller at elevated temperatures than the contribution due to lattice vibrations, and thus may be omitted in a simplified analysis. However, in more detailed quantitative description of the heat capacity data of U_4OsGe_8, the Schottky term should be taken into account.

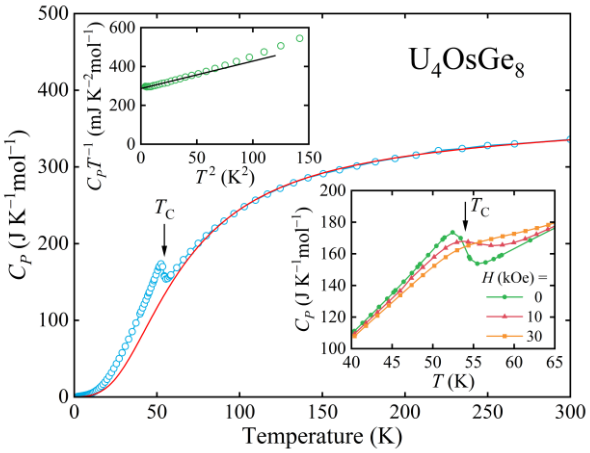

Figure 7 Temperature dependence of specific heat C_P of U_4OsGe_8; solid curve is a fit of Eq. (2) to the experimental data (see the text for details). Upper inset shows low-temperature C_P/T vs. T^2; solid line is a fit of Eq. (3) to the experimental data. Lower inset displays C_P(T) measured near T_C in various magnetic fields.

The Sommerfeld coefficient and the Debye temperature of U_4OsGe_8 can also be estimated from the low temperature, linear part of C_P/T plotted as a function of T^2 (see the upper inset to Fig.7), using the formula:

$$C_P = \gamma^{\mathrm{LT}} T + \beta T^3, \qquad (3)$$

where the first term is the electron contribution to the specific heat, and the second term represents the Debye model of acoustic lattice vibrations with the coefficient β:

$$\beta = \frac{1944r}{\left(\Theta_D^{\mathrm{LT}}\right)^3}$$

(the superscript LT means that this time the low-temperature range of $C_P(T)$ is taken into account). The least-squares fit of Eq. (3) to the experimental data (see the solid line in the upper inset to Fig.7) yielded the parameters γ^{LT} = 286 mJ K^{-2} mol^{-1} (viz. about 72 mJ K^{-2} mol$_U^{-1}$) and Θ_D^{LT} = 261 K.

As seen, the values of Θ_{D} obtained in the low-temperature range are consistent with those obtained in the high-temperature range. The Debye temperature is close to the values reported for the other U*TE*$_{1-x}$Ge$_2$ compounds [17,22,24] and has a magnitude characteristic of intermetallic compounds. The Sommerfeld coefficient obtained at low *T* is moderately enhanced and close to its values found in UNi$_{1-x}$Ge$_2$ (about 54 mJ K^{-2} mol$_U^{-1}$ [22]), in URu$_{1-x}$Ge$_2$ (about 61 mJ K^{-2} mol$_U^{-1}$ [24]) and in UFe$_{1-x}$Ge$_2$ (about 123 mJ K^{-2}mol^{-1} [17]). For the sake of comparison, it is worth recalling here that the value of the Sommerfeld coefficient determined for the structurally-related UGe$_2$ is equal to 34 mJ K^{-2} mol^{-1} [16], which is about two or four times smaller than that obtained for the ternary germanides. Such enhancement of γ in U-based intermetallics is often attributed to the presence of strong electron correlations between *5f* electrons and conduction band electrons, but here (*i.e.* in the U*TE*$_{1-x}$Ge$_2$ compounds) there is a clear tendency for γ to increase as the ordering temperature decreases, which might suggest that the γ value is enlarged (at least to some extent) by the magnons contribution to the specific heat.

The ferromagnetic phase transition in U$_4$OsGe$_8$ manifests itself as a pronounced λ-shaped anomaly located just below T_C. As can be inferred from the lower inset to Fig. 7, when magnetic field is applied, the anomaly shifts toward higher temperatures and blurs, as expected for ferromagnetic materials.

Conclusions

Our discovery that the compound known as structurally disordered URu$_{0.25}$Ge$_2$ is in fact the ordered system U$_4$RuGe$_8$ crystallizing with a much larger unit cell than postulated previously, sheds entirely new light on its physical properties, as well as those of other phases of the U*TE*$_{1-x}$Ge$_2$ family of compounds. In particular, the electrical resistivity of the Ru-bearing system can no longer be considered as influenced by the strong crystallographic disorder. Obviously, such a conclusion is also true for the novel phase reported here, namely U$_4$OsGe$_8$. The role of the crystallographic disorder in the Ni-bearing phases, in which formation of the superstructure has been ruled out by TEM experiments [23], and whose electrical resistivity shows quite similar features to those in the ordered compounds with Ru and Os, remains an open question. Similarly, the moderately enhanced electron contribution to the specific heat of the U*TE*$_{1-x}$Ge$_2$ compounds should not be attributed to the

crystallographic disorder, which is present only in some phases of this family. Rather, the specific heat data already collected for the four compounds (i.e. with Ru, Os, Fe and Ni) suggest that the observed Sommerfeld coefficient enhancement is likely related to magnon contribution to the specific heat of these phases.

Acknowledgements

This work was supported by the Polish National Agency for Academic Exchange NAWA (Warsaw, Poland, project no. PPN/BFR/2020/1/00022/U/00001) and Campus France (Paris, France, project no. 46871QL) within the PHC Polonium program. The authors from Rennes are grateful to ISCR-UMR6226 and ScanMat-UAR2025 directorates for the funding of a "projet Inter-UMR" in 2021-2022. The authors are grateful to the THEMIS platform (ScanMAT, UAR2025 University of Rennes 1-CNRS; CPER-FEDER 2007–2014) for performing TEM experiments. The synchrotron experiments were performed at Soleil, France, within "BAG for single crystal X-ray diffraction" proposal no. 20191503 on CRISTAL/4-Circles Diffractometer (for single crystals).

References

[1] M. S. Henriques, D. Berthebaud, J. C. Waerenborgh, E. B. Lopes, M. Pasturel, O.Tougait, A. P. Gonçalves, *A novel ternary uranium-based intermetallic $U_{34}Fe_{4-x}Ge_{33}$: structure and physical properties*, J. Alloys Compd., 606 (2014) 154-163. https://doi.org/10.1016/j.jallcom.2014.03.189

[2] M. S. Henriques, D. Berthebaud, L. C. J. Pereira, E. B. Lopes, M. B. C. Branco, H. Noël, O.Tougait, E. Santava, L. Havela, P. A. Carvalho, A. P. Gonçalves, *Structural and physical properties of the $U_9Fe_7Ge_{24}$ uranium germanide*, Intermetallics, 19 (2011) 841-847. https://doi.org/10.1016/j.intermet.2010.12.004

[3] S. F. Matar, V. Eyert, A. Mavromaras, S. Najm, B. Chevalier, J. Etourneau, *Chemical bonding and magnetism in the ternary germanides UT_2Ge_2 (T = 3d transition metal) from local spin density functional calculations*, J. Magn. Magn. Mater., 174 (1997) 219-235. https://doi.org/10.1016/S0304-8853(97)00147-9

[4] A. Soudé, O. Tougait, M. Pasturel, D. Kaczorowski, H. Noël, T. Roisnel, *Characterization of the novel intermetallic compounds U_2Co_3Ge, $U_6Co_{12}Ge_4$ and $U_6Co_{12}Ge_4C$*, J. Alloys Compd., 509 (2011) 5447-5452. https://doi.org/10.1016/j.jallcom.2011.02.094

[5] A. Soudé, O. Tougait, M. Pasturel, D. Kaczorowski, H. Noël, *Crystal structure and electronic properties of the new compounds $U_3Co_{12-x}X_4$ with X = Si, Ge*, J. Solid State Chem., 183 (2010) 1180-1185. https://doi.org/10.1016/j.jssc.2010.03.015

[6] B. Lloret, B. Buffat, B. Chevalier, J. Etourneau, *Structural, magnetic and electrical properties of some uranium ternary germanides: URh_2Ge_2, UIr_2Ge_2 and $U_4Ru_7Ge_6$, $U_4Os_7Ge_6$*, J. Magn. Magn. Mater., 67 (1987) 232-238. https://doi.org/10.1016/0304-8853(87)90236-8

[7] Y. Onuki, I. Ukon, S. W. Yun, I. Umehara, K. Satoh, T. Fukuhara, H. Sato, S. Takayanagi, M. Shikama, A. Ochiai, *Magnetic and electrical properties of U-Ge intermetallic compounds*, J. Phys. Soc. Jpn., 61 (1992) 293-299. https://doi.org/10.1143/JPSJ.61.293

[8] P. Boulet, G. M. Gross, G. André, F. Bourée, H. Noël, *Crystal and magnetic structure of new ternary uranium intermetallics: U_3TiX_5 (X = Ge,Sn)*, J. Solid State Chem., 144 (1999) 311-317. https://doi.org/10.1006/jssc.1999.8149

[9] M. S. Henriques, D. I. Gorbunov, J. C. Waerenborgh, M. Pasturel, A. V. Andreev, M. Dusek, Y. Skourski, L. Havela, A. P. Gonçalves, *Synthesis and structural/physical properties of $U_3Fe_2Ge_7$: a single-crystal study*, Inorg. Chem., 54 (2015) 9646-9655. https://doi.org/10.1021/acs.inorgchem.5b01736

[10] D. Kaczorowski, H. Noël, M. Potel, *Structural, magnetic and electrical properties of new uranium intermetallics: $U_3Cu_4Si_4$ and $U_3Cu_4Ge_4$*, Physica B, 206-207 (1995) 457-460. https://doi.org/10.1016/0921-4526(94)00489-I

[11] S. K. Dhar, K. V. Shah, P. Bonville, P. Manfrinetti, F. Wruble, *Structure and magnetic properties of U_2Fe_3Ge*, Solid State Commun., 147 (2008) 217-220. https://doi.org/10.1016/j.ssc.2008.05.016

[12] M. S. Henriques, D. I. Gorbunov, J. C. Waerenborgh, L. Havela, A. B. Shick, M. Divis, A. V. Andreev, A. P. Gonçalves, *Unusual 5f magnetism in the U_2Fe_3Ge ternary Laves phase: a single crystal study*, J. Phys.:Cond. Matter, 25 (2013) 066010. https://doi.org/10.1088/0953-8984/25/6/066010

[13] S. S. Saxena, P. Agarwal, K. Ahilan, F. M. Grosche, R. K. W. Haselwimmer, M. J. Steiner, E. Pugh, I. R. Walker, S. R. Julian, P. Monthoux, G. G. Lonzarich, A. Huxley, I. Sheikin, D. Braithwaite, J. Flouquet, *Superconductivity on the border of itinerant-electron ferromagnetism in UGe_2*, Nature, 406 (2000) 587-592. https://doi.org/10.1038/35020500

[14] N. T. Huy, A. Gasparini, D. E. de Nijs, Y. Huang, J. C. P. Klaasse, T. Gortenmulder, A. de Visser, A. Hamann, T. Gorlach, H. von Lohneysen, *Superconductivity on the border of weak itinerant ferromagnetism in UCoGe*, Phys. Rev. Lett., 99 (2007) 067006. https://doi.org/10.1103/PhysRevLett.99.067006

[15] D. Aoki, A. Huxley, E. Ressouche, D. Braithwaite, J. Flouquet, J.-P. Brison, E. Lhotel, C. Paulsen, *Coexistence of superconductivity and ferromagnetism in URhGe*, Nature, 413 (2001) 613-616. https://doi.org/10.1038/35098048

[16] D. Aoki, K. Ishida, J. Flouquet, *Review of U-based ferromagnetic superconductors: comparison between UGe_2, URhGe, and UCoGe*, J. Phys. Soc. Jpn., 88 (2019) 022001. https://doi.org/10.7566/JPSJ.88.022001

[17] M. Szlawska, M. Pasturel, D. Kaczorowski, A. Pikul, *Ferromagnetism in structurally disordered $UFe_{0.39}Ge_2$*, J. Alloys Coumpounds, 892 (2021) 162032. https://doi.org/10.1016/j.jallcom.2021.162032

[18] A. Pikul, R. Idczak, P. Sobota, W. Nowak, M. Pasturel, V. H. Tran, *Ferromagnetic ordering in $UFe_{0.40}Ge_2$ studied by ^{57}Fe Mössbauer spectroscopy*, J. Magn. Magn. Mater. 553 (2022) 169238. https://doi.org/10.1016/j.jmmm.2022.169238

[19] A. Soudé, *Caractérisations chimiques structurales et électroniques des phases intermétalliques (Ce,U)-Co-Ge*, PhD thesis, Université de Rennes 1 (2010).

[20] Z. Molcanova, M. Mihalik, M. Mihalik Jr., M. Reiffers, A. Dzubinska, M. Hurakova, V. Kavecansky, M. Paukov, L. Havela, *Charactrization of the new U-Ni-X_2 splats and study of their physical properties*, Acta. Phys. Pol. A, 131 (2017) 994-996. https://doi.org/10.12693/APhysPolA.131.994

[21] K. Ohashi, M. Ohashi, M. Sawabu, M. Miyagawa, K. Maeta, T. Yamamura, *Magnetic properties of the $UNiGe_2$ at low temperature*, J. Phys.:Conf. Ser., 969 (2018) 012101. https://doi.org/10.1088/1742-6596/969/1/012101

[22] M. Pasturel, M. Szlawska, J. Ćwik, D. Kaczorowski, A. Pikul, *Antiferromagnetic ordering in the ternary uranium germanide $UNi_{1-x}Ge_2$: neutron diffraction and physical properties studies*, Intermetallics 131 (2021) 107112. https://doi.org/10. 1016/j.intermet.2021.107112

[23] A. P. Pikul, M. Szlawska, X. Ding, J. Sznajd, M. Ohashi, D. A. Kowalska, M. Pasturel, K. Gofryk, *Competition of Magnetocrystalline Anisotropy of Uranium Layers and Zig-Zag Chains in $UNi_{0.34}Ge_2$ Single Crystals*, accepted to Phys. Rev. Materials, https://arxiv.org/abs/2206.03397

[24] M. Pasturel, A. Pikul, G. Chajewski, Noël, D. Kaczorowski, *Ferromagnetic ordering in the novel ternary uranium germanide $URu_{0.29}Ge_2$*, Intermetallics 95 (2018) 19. https://doi.org/10.1016/j.intermet.2018.01.011

[25] M. A. Zhuravleva, D. Bilc, R. J. Pcionek, S. D. Mahanti, M. G. Kanatzidis, *Tb_4FeGe_8 grown in liquid gallium: trans-cis chains from the distorsion of a planar Ge square net*, Inorg. Chem., 44 (2005) 2177-2188. https://doi.org/10.1021/ic0487878

[26] J. L. Zhang, Y. M. Wang, S. Bobev, *Structural modulations in the rare-earth metal digermanides $REAl_{1-x}Ge_2$ (RE = Gd-Tm, Lu, Y; 0.8 < x < 0.9). Correlations between long- and short-range vacancy ordering*, Inorg. Chem., 54 (2015) 722-732. https://doi.org/10.1021/ic501002j

[27] J. K. Bao, H. H. Zheng, J. G. Wen, S. Ramakrishnan, H. Zheng, J. S. Jiang, D. Bugaris, G. Cao, D. Y. Chung, S. van Smaalen, M. G. Kanatzidis, *Superconductivity in Y_4RuGe_8 with a vacancy-ordered $CeNiSi_2$-type structure*, Chem. Mater., 33 (2021) 7839-7847. https://doi.org/10.1021/acs.chemmater.1c02488

[28] S. D. Nguyen, K. Ryan, P. Chai, M. Shatruk, Y. Xin, K. W. Chapman, P. J. Chupas, F. R. Fronczek, R. T. Macaluso, *$Pr_{1.33}Pt_4Ga_{10}$: superstructure and magnetism*, J. Solid State Chem., 220 (2014) 9-16. https://doi.org/10.1016/j.jssc.2014.07.033

[29] F. Weill, M. Pasturel, J.-L. Bobet, B. Chevalier, *Ordering phenomena in intermetallic CeMX (M = Ni, Cu and X = Si, Ge, Sn) upon hydrogenation*, J. Phys. Chem. Solid., 67 (2006) 1111-1116. https://doi.org/10.1016/j.jpcs.2006.01.032

[30] J. L. Zhang, Y. Y. Liu, C. H. Shek, Y. M. Wang, S. Bobev, *On the structure of the rare-earth metal germanides from the series $REAl_{1-x}Ge_3$ (RE = Nd, Sm, Gd, Tb, Dy, Ho; 0.6 < x < 0.9). A tale of vacancies at the Al sites and the concomitant structural modulations*, Dalton Trans., 46 (2017) 9253-9265. https://doi.org/10.1039/c7dt01977g

[31] J. Rodriguez-Carvajal, *Recent advances in magnetic-structure determination by neutron powder diffraction*, Physica B, 192 (1993) 55-69. https://doi.org/10.1016/0921-4526(93)90108-I

[32] L. Palatinus, G. Chapuis, *SUPERFLIP – a computer program for the solution of crystal structures by charge flipping in arbitrary dimensions*, J. Appl. Crystallogr., 40 (2007) 786-790. https://doi.org/10.1107/S0021889807029238

[33] V. Petříček, M. Dušek, L. Palatinus, *Crystallographic computing system JANA2006: General features*, Z. Kristallogr., 229 (2014) 345–352. https://doi.org/10.1515/zkri-2014-1737

[34] E. Parthé, K. Cenzual, R. Gladyshevskii, *Standardization of crystal structure data as an aid to the classification of crystal-structure types*, J. Alloys Compd., 197 (1993) 291-301. https://doi.org/10.1016/0925-8388(93)90049-S

[35] C. Prestipino, URL:https://github.com/Prestipino/TEMpcPlot, visited on 2022/10/04.

[36] R. Troć, Z. Gajek, A. Pikul, *Dualism of the 5f electrons of the ferromagnetic superconductor UGe_2 as seen in magnetic, transport, and specific-heat data*, Phys. Rev. B, 86 (2012) 224403. https://doi.org/10.1103/PhysRevB.86.224403

[37] R. Troć, H. Noël, P. Boulet, *Magnetotransport of compounds in the U-Ge system*, Phil. Mag., 82 (2002) 805-824. https://doi.org/10.1080/13642810208224371